Journal Name

COMMUNICATION

# Dual Photonic-Bandgap Optical Films towards Generation of Photonic Crystal-Derived 2-Dimensional Chemical Codes

Received 00th January 20xx,
Accepted 00th January 20xx

DOI: 10.1039/x0xx00000x

www.rsc.org/

Jing Zhang,[a] Shengyang Yang,[a] Yu Tian,[a] Cai-Feng Wang,[a] and Su Chen*[a]

**A chemical-oriented 2-Dimensional (2D) optical code was first time constructed by integrating bi-layer or bistriate-structure responsive photonic crystals (RPCs), which not only represents high information capacity in encoding processes, but offers a facile route towards high performance sensors along with both accurate analysis and anti-jamming performances.**

Today, two-dimensional (2D) barcodes are extensively exploited as quick response codes for industrial uses, especially in e-business field. Inspired by the commercial 2D barcodes, we expect to design a chemical-oriented 2D optical code by integrating bilayer or bistriate-structrure responsive photonic crystals (RPCs), which would offer chemicals with their own characteristic codes for the first time.

Up to now, RPCs with easy-to-read and self-reporting traits have aroused great interests due to their unique light manipulation and inhibition capabilities in areas ranging from displays,[1, 2] inks and paints,[3] to various chemical/biological sensors.[4,5] Because different molecules normally lead to diverse optical signals namely the photonic bandgaps (PBGs), the recognition of specific molecules can thus be realized. Typically, diverse 3-dimensional macroporous films with inverse opal structures were developed to distinguish various solvents based on the corresponding value of average refractive index (RI).[6] To further increase the selectivity and sensitivity of RPCs, specific functional hydrogels had been introduced to detect target analytes.[7] Moreover, a series of reliable RPC-based sensors were also put into practice via improving their chemical resistivity and physical rigidity.[8] Despite great advance has been attained, most of previous approaches mainly focused on single signal monitor, leading to low information densities and difficulties in sensing under interference environment.

Herein, we first time demonstrate a 2D optical code containing bilayer or bistriate-structure RPCs towards chemical encoding and

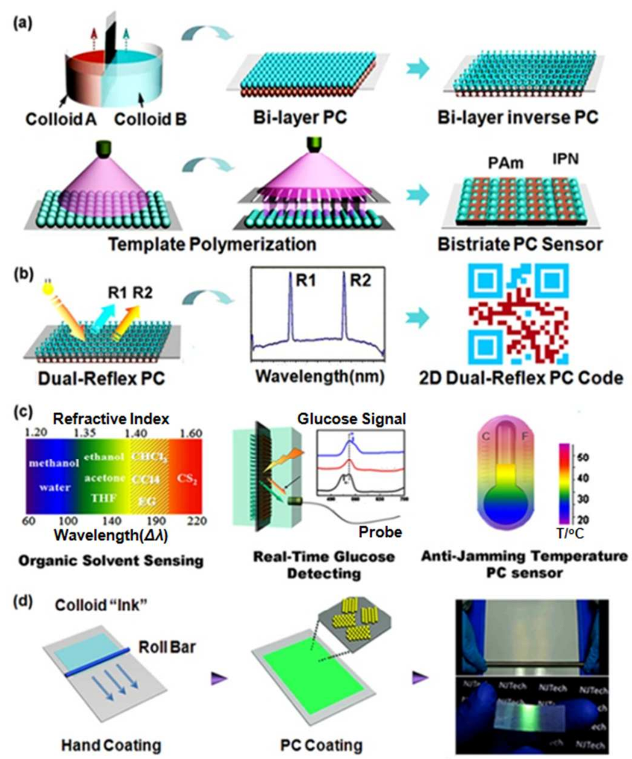


**Scheme 1** a) Schematic illustration of the fabrication processes for 2D optical codes from bi-layer or bistriate RPCs. b) The forming mechanism of dual-PBG signals for the 2D optical code. c) The applications of the 2D optical code, involving organic solvent encoding, real-time glucose detecting, and anti-interference thermal sensing. d) Scaled-up production of the RPC-derived 2D optical codes on flexible substrates via hand coating.

sensing applications (Scheme 1a). Just as the timing and finder pattern design in commercial 2D barcodes, the 2D optical code successfully integrates double monitor signals into a single unit: one reflex peak serves as control signal, the other one is as recognition signal, and their superposition $\Delta\lambda$ expresses final sensing information (Scheme 1b). These features not only enable the 2D optical code to translate more chemical messages in encoding processes but offer an alternative access to real-time and accurate chemical sensing under interference environment. Accordingly,

[a] State Key Laboratory of Materials-Oriented Chemical Engineering and College of Chemistry and Chemical Engineering. NanjingTech University (former Nanjing University of Technology), 5 Xin Mofan Road, Nanjing 210009, P. R. China. E-mail: chensu@njtech.edu.cn

† Electronic Supplementary Information (ESI) available: Reagents and instruments, experimental procedures, formula derivation, additional figures and videos. See DOI: 10.1039/x0xx00000x

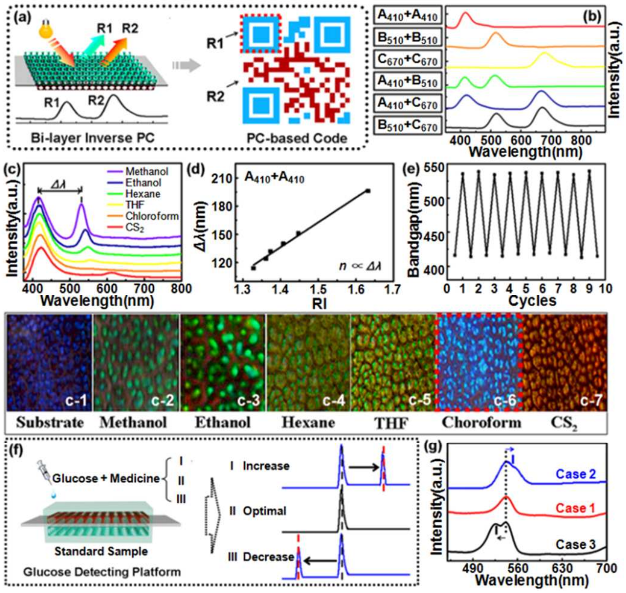


**Fig. 1** a) Schematic formation of bilayer-structure 2D optical code. b) Reflection spectra of some typical 2D optical codes. c) A typical $A_{410}$+$A_{410}$-typed 2D code used for encoding the selected solvents with increasing RI: methanol (n=1.329), ethanol (n=1.360), hexane (n=1.375), tetrahydrofuran (THF) (n=1.407), chloroform (n=1.473), and carbon disulfide ($CS_2$) (n=1.630), and their corresponding microscope images(C-1, C-2, to C-7). d) The relationship between wavelength internals and the RI of the filling liquids in solvent encoding. e) The cycling performance of the resulting 2D optical code with ethanol. f) The set-up for real-time glucose detecting with the 2D optical code and its building mechanism. g) The practical application of the 2D PC code in real-time glucose detection.

diverse optical devices were successfully established toward organic solvent recognition, real-time glucose detection, and anti-interference thermal sensing (Scheme 1c). Furthermore, we also designed a kind of PS latice bearing with hard-core/soft-shell structures, allowing them to be easily coated on flexible substrates including papers and plastics, and then producing a series of robust flexible 2D optical codes with tunable PBG signals, which would undoubtedly facilitate the resulting 2D optical codes to commercial uses (Scheme 1d).

Herein, the bilayer-structure 2D optical codes were constructed via a template method (Fig. S1). As the reflex peak originating from the bottom layer of the resulting 2D optical code film can be detected when the top layer is sufficiently thin (Fig. S2), diverse optical code series with different dual PBG signals can thus be achieved by tuning the colloid template sizes (Fig. 1a). The typical spectra codes are listed in Fig. 1b, where the peak of the spectra code strings is denoted by alphabets, such as A, B and C, while the followed number indicates the specific wavelength of PBG. For instance, $A_{410}$, $B_{510}$, $C_{670}$ indicate the optical code series with PBGs at ca. 410, 510, and 670 nm, derived from the colloid templates with diameter of 266, 315, and 420 nm, respectively (Fig. S3). When the top and bottom sides of the bilayer-structure RPCs are the same, such as $A_{410}$+$A_{410}$, $B_{510}$+$B_{510}$, and $C_{670}$+$C_{670}$, only single reflex peak could be noticed (Fig. 1b). However, when the two layers are constructed from different colloid templates, two distinctive reflex peaks are realized, which enables to translate more spectra code information into the 2D optical codes compared to the conventional single reflex RPC materials.

Using the bilayer-structure RPCs as the 2D optical code, for the first time, we offered various organic solvents with their own characteristic spectra codes. Fig. 1c shows the specific spectra of the $A_{410}$+$A_{410}$-typed code sequentially infused with the diverse solvents with increasing RI (Table S1). The shift wavelength ($\Delta\lambda$) and the maximum intensity of the reflex peak in the presence of different solvents change along with the increase of solvent RI ($n_{solvent}$) (Fig. S4). In particular, a linear correlation between $\Delta\lambda$ and $n_{solvent}$ is noted (Fig. 1d), which is in good agreement with the derived formula (See Supporting Information):[9, 10]

$$\Delta\lambda = \lambda - \lambda_0 = (2d/m)(1-\Phi)n_{solvent} + (2d/m)\Phi n_{silica} - \lambda_0$$

where $\lambda$ and $\lambda_0$ denote the sensing and control reflex peak positions, respectively, $d$ is the spacing between close-packed planes of voids, $m$ is the order of Bragg diffraction, $\Phi$ is the solid fraction of the inverse RPC, and $n_{silica}$ is the RI of the silica wall. Also, these 2D RPC codes show distinctive color changes during the encoding processes, varying from blue (the blank sample, C-1) to blue-green (methanol, C-2), green (ethanol, C-3), yellowish-green (hexane, C-4), yellow (tetrahydrofuran, C-5), bright blue(chloroform, C-6), and orange (carbon disulfide, C-7). This feature shows the possibility for encoding various chemical solvents with the dual-PBG optical code, and even judging by visual observation. Additionally, the cyclical encoding and decoding processes reveal that the optical codes of the homologous position almost remain consistent for more than nine cycles, demonstrating their reliability in durative practical use (Fig. 1e).

The dual PBG traits also endow the 2D optical code with advantages for real-time monitoring applications. As the left part of Fig. 1f shows, an in-situ glucose monitoring system, with synchronous optical signals from the control (bottom) and sensing (top) layers of the 2D optical code, is set up. The concentration changes of the glucose can thus be directly recognized based on the wavelength intervals (Fig. S5). More attractively, when the control layer of the 2D optical code is immersed by the standard glucose sample, the concentration deviation of the sensing glucose solution from standard state can thus be distinguished (the right part of Fig. 1f). In order to take an example, a series mass concentration, 5%, 35%, and 50% of glucose samples and a standard control sample with the glucose mass concentration of 35% were utilized for concretely implementing our scheme (Fig. 1g and Table S2). It can be seen that, when the concentration of the sensing glucose sample approximates to that of the standard sample, the 2D RPC code displays overlapped optical signals due to similar RI values (Case 1). However, when the concentration of the sensing sample has a considerable departure from the standard state, the peak separation behaviour happens (Case 2 and Case 3). Through analysis of their relative positions, we can facilely conclude the variation tendency, which eliminates the need for original state recording and greatly simplifies the analysis and judgement processes comparing to conventional single reflex RPCs. Although, when the sensing and standard samples have close concentration values, the broad sensing and control peaks tends to be merged, thus leading to the difficulty in telling the exact extent of concentration deviation, this feature is still applicable in a wide variety of situations. For example, the optimal conditions normally span a broad range in strains breeding, and regulation is necessary only when the situation get seriously far out of the standard state.

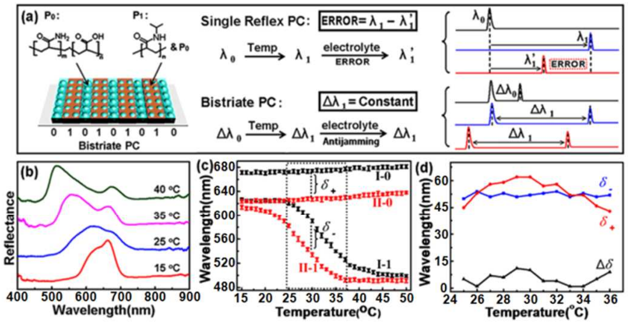


**Fig. 2** a) Schematic illustration for the construction of the bistriate 2D optical code and their sensing mechanism. b) The typical reflex spectra for the bistriate 2D optical code at 15, 25, 35 and 40 °C. c) The effects of the temperature on reflex peak position of Bistriate 0 and Bistriate 1 at varied temperature: Curve I-0 and Curve I-1 correspond to the detailed reflex peak position in Bistriate 0 and Bistriate 1 at varied temperature without salt addition, while Curve II-0 and Curve II-1 corresponds to the results in a solution containing 100 ppm NaCl. d) The deviation degree of the peak signal for Bistriate 0 ($\delta_-$), Bistriate 1 ($\delta_+$) and the bistriate 2D optical code ($\Delta\delta$).

Thus, an alternative feedback platform with quick and simple signal expressions is successfully established for these cases.

More significantly, the 2D optical codes were also applicable to sensing under interference environment. Accordingly, a bistriate 2D optical code incorporated with acrylamide (Am) and acrylic acid (AA) components was first time established for anti-jamming thermal response (Fig. S6). Equally, due to the periodically varied compositions, dual-PBG signals were attained. The NIPAm-incorporated regions (denoted as Bistriate 1) confer thermo-sensitivity to the bistriate 2D optical code (Fig. 2a). As indicated in Fig. 2b, its reflex peak from Bistriate 1 shifts to blue along with the increase of temperature due to the decreased lattice spacing caused by the hydrophilic-to-hydrophobic transition of poly-NIPAm gels. However, the reflex peak from AA regions (denoted as Bistriate 0) remains nearly the same while the temperature is rising. Therefore, the temperature deviation can be directly recognized based on the wavelength interval. More interestingly, the bistriate 2D optical code-based thermo-sensor also exhibited good performance in interference suppression. As seen in Fig. 2c, Curve I-0 and I-1 show the reflex peak from Bistriate 0 and Bistriate 1 in pure water at varied temperature. In contrast, Curve II-0 and II-1 presents the corresponding results conducted in a solution containing 100 ppm NaCl. It can be seen that once trace amount of salt existed in the solution, the reflex peak positions demonstrate obviously blue-shift for both Bistriate 0 and Bistriate 1. However, the blue-shift amount reveals close value at the temperature range from 25 to 36 °C, and the measurement deviation ($\Delta\delta$) can thus be evidently narrowed by:

$$\Delta\delta = |\delta_+ - \delta_-|$$

where $\delta_+$ and $\delta_-$ refer to the signal derived from Bistriate 1 and Bistriate 0, respectively (Fig. 2d). Consequently, a variation compensation scheme is successfully set up here by the bistriate 2D optical code, benefiting to enhance error correction capability and improve the sensing accuracy. To the best of our knowledge, it is the first example of the utilization of hydrogel-based dual-PBG code film in preparation of anti-jamming RPC sensors, allowing an alternative access to high-accuracy sensors.[11, 12] Moreover, considering that the temperature rang is suitable for living beings, and it may find potential applications in biological areas.

In addition, the construction of flexible 2D optical codes on various substrates (e.g. paper, flexible plastic film) was also conducted, which would undoubtedly facilitate their practical uses. As shown in Fig. 3a, to enhance the adhesion between the 2D optical code and flexible substrates including papers and plastics, monodispersed lattices with hard-core/soft-shell structures were first prepared by grafting the polystyrene (PS) seed microspheres with acrylic resins (Fig. S7). Fig. 3b shows the optical image of the as-obtained lattice film without obvious cracks, implying the improved connectivity between the resin-grafted latices. The corresponding infrared image of core/shell latices is presented in Fig. 3c. Compared to the infrared image of PS spheres (Fig. 3d), an obviously improved intensity at 1,732 $cm^{-1}$ was noted, indicating the existence of soft resin fragments (Fig. S8). Also, a decreased thermal stability was found after the grafted polymerization, which further confirmed the successful incorporation of soft acrylic resins (Fig. S9). These monodispersed lattices with hard-core/soft-shell

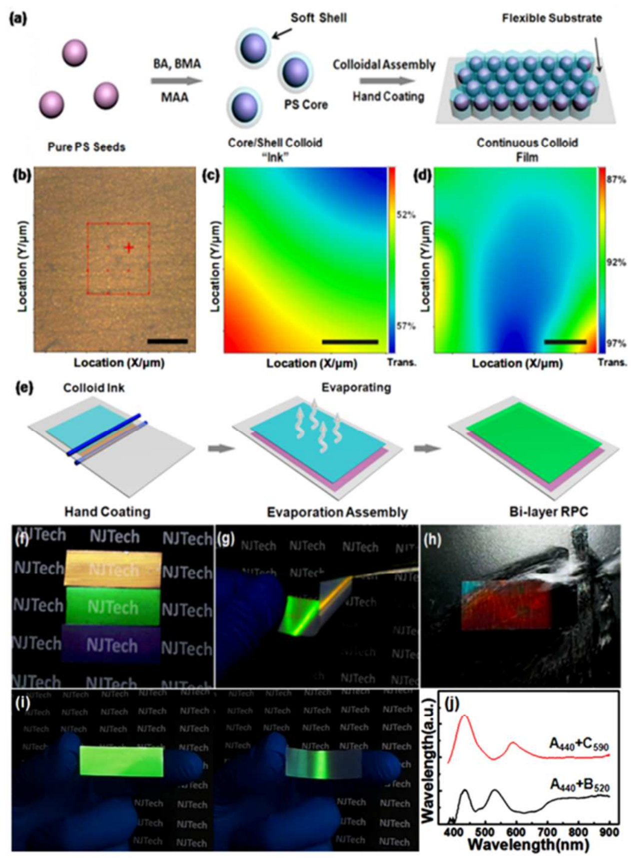


**Fig. 3** a) Schematic illustration for the construction of flexible 2D optical code films via hand print. b) The microscopic image of the opal film constructed by hard-core/soft-shell PS colloids. c, d) The infrared chemical images of the hard-core/soft-shell PS colloids and the pure PS colloids. e) The detailed hand coating process for creating optical code films on flexible substrates. f) The optical image of the code films constructed by the hard-core/soft-shell PS latices on Au substrate. g) The code film with dual PBG signals prepared by repeating hand print. h) The film rinsed by fresh water to test its water resistance. i) Bend the film to test its stability and flexibility. j) The spectra series of 2D RPC codes on flexible PETs. Scale bar 50 μm.

structures can be facilely assembled onto various substrates such as polyethylene terephthalate (PET) and paper within 5 min via hand print (Video S1), allowing large scale preparation of the flexible 2D optical codes (Fig. 3e). Besides, these 2D optical code films still kept highly ordered structures (Fig. S10) and presented bright structural colours. By tuning the colloid size, a series of optical code films with different structural colours ranging from red, green to blue were obtained (Fig. 3f). Also, these films showed superior stability under rinse of water (Fig. 3h and Video S2), and could be bent like folded screens (Fig. 3i and Video S3). Moreover, in virtue of the transparency of the RPC layer (Fig. S11), dual PBG singals could also be achieved (Fig. 3g) on various flexible substrates for the development of diverse encoded spectrum series (Fig. 3j). These traits would greatly extend the 2D optical codes to large-scale practical applications in areas containing coatings, bio-encoding, and displays.

In summary, we demonstrate an operable strategy for the construction of chemical-oriented 2D optical code containing bi-layer or bistriate-structure RPCs, which extend photonic crystals to be a candidate of 2D code materials for chemical recognition for the first time. These 2D RPC codes successfully integrate dual reflex peak signals into a single material, and thus they not only represent more information capacity in encoding process, but offer a facile route towards high precise and anti-jamming detection. Perhaps more interestingly, we have taken the example for creating a series of robust flexible film materials with 2D optical codes on a large scale by using as-prepared hard-core/soft-shell lattices. More practical applications of 2D RPC code materials, such as chemical sensing, anti-counterfeiting and flexible displays, will continue.

This work was supported by National Natural Science Foundation of China (21076103), Industrial Project in the Science and Technology Pillar Program of Jiangsu Province (BE2012181), and Priority Academic Program Development of Jiangsu Higher Education Institutions (PAPD).

## Notes and references

1 a) A. C. Arsenault, D. P. Puzzo, I. Manners and G. A. Ozin, *Nat. Photon.*, 2007, **1**, 468; b) H. Gu, Y. J. Zhao, Y. Cheng, Z. Y. Xie, F. Rong, J. Q. Li, B. P. Wang, D. G. Fu and Z. Z Gu, *small*, 2013, **9**, 2266; c) H. Li, J. Wang, H. Lin, L. Xu, W. Xu, R. Wang, Y. Song and D. Zhu, *Adv. Mater.*, 2010, **22**, 1237; d) K. Hwang, D. Kwak, C. Kang, D. Kim, Y. Ahn and Y. Kang, *Angew. Chem. Int. Ed.*, 2011, **50**, 6311.

2 a) Z. Y. Yu, C. F. Wang, L. Ling, L. Chen and S. Chen, *Angew. Chem. Int. Ed.*, 2012, **51**, 2375; b) S. N. Yin, C. F. Wang, Z. Y. Yu, J. Wang, S. S. Liu and Su Chen, *Adv. Mater.*, 2011, **23**, 2915; c) Q. Fu, A. Chen, L. Shi and J. Ge, *Chem. Commun.*, 2015, **51**, 7382.

3 a) H. Kim, J. Ge, J. Kim, S. Choi, H. Lee, H. Lee, W. Park, Y. Yin and S. Kwon, *Nat. Photon.*, 2009, **3**, 534; b) S. H. Kim, H. Hwang and S. M. Yang, *Angew. Chem. Int. Ed.*, 2012, **51**, 3601; c) H. Y. Ko, J. Park, H. Shin and J. Moon, *Chem. Mater.*, 2004, **16**, 4212.

4 a) D. Xu, W. Zhu, C. Wang, T. Tian, J. Li, Y. Lan, G. Zhang, D. Zhang and G. Li, *Chem. Commun.*, 2014, **50**, 14133; b) J. E. Stumpel, D. J. Broer and A. P. H. J. Schenning, *Chem. Commun.*, 2014, **50**, 15839; c) C. Fenzl, T. Hirsch and O. S. Wolfbeis, *Angew. Chem. Int. Ed.*, 2014, **53**, 3318; d) X. Li, L. Peng, J. Cui, W. Li, C. Lin, D. Xu, T. Tian, G. Zhang, D. Zhang and G. T. Li, *small*, 2012, **8**, 612.

5 a) M. Chen, L. Zhou, Y. Guan and Y. Zhang, *Angew. Chem. Int. Ed.*, 2013, **52**, 9961; b) B. Ye, H. Ding, Y. Cheng, H. Gu, Y. Zhao, Z. Xie and Z. Gu, *Adv. Mater.*, 2014, **26**, 3270; c) C. Zhang, G. G. Cano and P. V. Braun, *Adv. Mater.*, 2014, **26**, 5678; d) J. Ge and Y. Yin, *Angew. Chem. Int. Ed.*, 2011, **50**, 1492.

6 a) I. B. Burgess, L. Mishchenko, B. D. Hatton, M. Kolle, M. Lončar and J. Aizenberg, *J. Am. Chem. Soc.*, 2011, **133**, 12430; b) H. Li, L. Chang, J. Wang, L. Yang and Y. Song, *J. Mater. Chem.*, 2008, **18**, 5098.

7 a) W. Hong, X. Hu, B. Zhao, F. Zhang and D. Zhang, *Adv. Mater.*, 2010, **22**, 5043; b) T. Kanai, D. Lee, H. C. Shum, R. K. Shah and D. A. Weitz, *Adv. Mater.*, 2010, **22**, 4998; c) J. H. Holtz and S. A. Asher, *Nature*, 1997, **389**, 829.

8 a) D. Yang, Y. Qin, S. Ye and J. Ge, *Adv. Funct. Mater.*, 2014, **24**, 817; b) S. H. Kim, J. G. Park, T. M. Choi, V. N. Manoharan and D. A. Weitz, *Nat. Commun.*, DOI 10.1038/ncomms4068; c) X. Meng, R. Al-Salman, J. Zhao, N. Borissenko, Y. Li and F. Endres, *Angew. Chem. Int. Ed.*, 2009, **48**, 2703.

9 a) C. F. Blanford, R. C. Schroden, M. Al-Daous and A. Stein, *Adv. Mater.*, 2001, **13**, 26; b) J. Zhang, L. Ling, C. F. Wang, S. Chen, L. Chen and D. Y. Son, *J. Mater. Chem. C*, 2014, **2**, 3610.

10 a) G. I. N. Waterhouse, J. B. Metson, H. Idriss and D. S. Waterhouse, *Chem. Mater.*, 2008, **20**, 1183; b) L. Wang, J. Wang, Y. Huang, M. Liu, M. Kuang, Y. Li, L. Jiang and Y. Song, *J. Mater. Chem.*, 2012, **22**, 21405.

11 a) Q. L. Tan, C. Li, J. J. Xiong, P. G. Jia, W. D. Zhang, J. Liu, C. Y. Xue, Y. P. Hong, Z. Ren and T. Luo, *Sensors*, 2014, **14**, 2417; b) F. B. John, M. A. Alejandro and T. Roberto, *Opt. Lett.*, 2014, **39**, 3074.

12 a) M. J. Sailor, *ACS Nano*, 2007, **1**, 248; b) A. M. Ruminski, M. M. Moore and M. J. Sailor, *Adv. Funct. Mater.*, 2008, **18**, 3418; c) Y. Cui, F. Zhu, B. Chen and G. Qian, *Chem. Commun.*, 2015, **51**, 7420.